Dalton Transactions



PERSPECTIVE

View Article Online
View Journal | View Issue



Cite this: *Dalton Trans.*, 2014, **43**, 17596

# A novel aspect of spectroscopy for porphyrinic compounds under magnetic fields

Yanyan Mulyana* and Kazuyuki Ishii*

The spectroscopies of a range of porphyrinic compounds performed under a magnetic field are reviewed, focusing on the molecular functions of the compounds. Characteristic molecular magneto-optical effects, such as the Kerr effects and magnetochiral dichroism (MChD), as well as time-resolved electron paramagnetic resonance (TREPR) are reviewed. A novel molecular magneto-optical memory is described on the basis of the results of a Kerr spectroscopic study of Si phthalocyanine coupled with a ferromagnetic substrate. The results of TREPR analyses of low-symmetry tetraazaporphyrin derivatives are discussed in order to determine the relationship between molecular symmetry and singlet oxygen yield, as knowing this relationship is essential for photodynamic therapy. Finally, the MChD of porphyrins is introduced as a new way of elucidating the asymmetry in biological systems. Further, it can lead to new asymmetric synthesis methods and form the basis for novel magneto-optical devices.

Received 14th May 2014,
Accepted 16th September 2014

DOI: 10.1039/c4dt01428f

www.rsc.org/dalton



## Introduction

Porphyrinic compounds have been the focus of extensive investigations for several decades. For instance, naturally occurring porphyrins such as chlorophylls and hemes have been studied widely in order to gain a better understanding of their biological roles.[1] Furthermore, synthetic porphyrins have been manipulated for use in a wide range of applications.[2–6]

The technological promise of porphyrinic compounds is associated with their photochemical properties, which are based on the absorption of light in the visible and near-infrared regions, namely, the characteristic π–π* transitions such as Soret and Q absorption bands, as well as the photochemical

*Institute of Industrial Science, The University of Tokyo, 4-6-1 Komaba, Meguro-ku, Tokyo 153-8505, Japan. E-mail: k-ishii@iis.u-tokyo.ac.jp, ymulyana@iis.u-tokyo.ac.jp*

**Yanyan Mulyana**

*Yanyan Mulyana earned a BSc in chemistry at Padjadjaran University, Indonesia, an MSc at the University of Sydney under the direction of Professor Leonard F. Lindoy and a PhD at the University of Melbourne under the supervision of Dr Colette Boskovic. In 2009, he undertook a postdoctoral fellowship with Professor F. Richard Keene at James Cook University, followed by a second postdoctoral fellowship with Professor Leone Spiccia at Monash University. In 2013, he was awarded a Japan Society for the Promotion of Science (JSPS) fellowship at the Institute of Industrial Science, University of Tokyo, under the mentorship of Professor Kazuyuki Ishii. His research interests include molecular magnetism, supramolecular chemistry, bioinorganic chemistry and artificial photosynthesis.*

**Kazuyuki Ishii**

*Kazuyuki Ishii earned his PhD in chemistry at Tohoku University in 1996 under the direction of Professor Seigo Yamauchi. From 1996 to 2006, he worked as a Research Associate in the laboratory of Professor Nagao Kobayashi at Tohoku University. In 2006, he took up the position of an Associate Professor at the Institute of Industrial Science, University of Tokyo, where he later became a full Professor in 2012. His research projects include the photofunctionalization of various metal complexes such as porphyrins, phthalocyanines, and their derivatives.*

reactions that occur *via* the lowest excited singlet ($S_1$) and triplet ($T_1$) states. Spectroscopies performed under a magnetic field, such as magneto-optical effects and electron paramagnetic resonance (EPR), have been well-known as useful methods for investigating the π–π* excited states of porphyrinic compounds.

Since spin–orbit coupling (SOC) is relatively weak in π–π* configurations, magnetic circular dichroism (MCD) spectroscopy, which is an analytical technique based on magneto-optical effects,[7] has been used in porphyrinic compounds for analysing the degeneracy of excited states and the orbital angular momentum between the excited states. Furthermore, using a time-resolved EPR (TREPR) technique, which is very useful for detecting the paramagnetic intermediate species of photoreactions, such as excited triplet states, several parameters, *i.e.*, the zero-field splitting (ZFS), the *g* values, and the excited-state spin dynamics, can be elucidated. Thus, spectroscopies performed under a magnetic field can offer unique information related to the orbital and spin angular momentums, and contribute to elucidating the electronic structures of porphyrinic compounds (Fig. 1).

Recently, with the increasing need for the functionalisation of molecules, several studies based on spectroscopic methods performed under a magnetic field have been reported not only for imparting novel functionalities to porphyrinic compounds but also for improving the range of their molecular design. This perspective presents some of the important highlights of spectroscopies performed under a magnetic field by concentrating on how such techniques can contribute to the functionalisation of molecules and clarify the roles of biological systems. The first example of a spectroscopy related to magneto-optical effects is the molecular Kerr spectroscopy of phthalocyanine thin films on ferromagnetic substrates. Using Kerr spectroscopy, a novel functionality, namely, a molecular magneto-optical memory, which can overcome the memory-capacity dependence on the diffraction limit of light, is proposed on the basis of the molecular magnetic hysteresis observed at room temperature. The second example is magneto-chiral dichroism (MChD), which can potentially help in elucidating the homochirality of life. The MChD of the π–π* excited states of porphyrin oligomers is described; this has significant advantages such as tunable wavelengths and high chemical reactivity, which are useful for the development of novel asymmetric synthesis methods and magneto-optical devices. It also opens up new possibilities for clarifying the asymmetry noticed in biological systems. Finally, from the viewpoint of the relationship between the ZFS and the singlet oxygen quantum yield ($\Phi_D$), TREPR is discussed using low-symmetry porphyrin analogues. Elucidating this relationship could allow for greater flexibility in the design of the singlet-oxygen generators used in photodynamic therapy (PDT).

## Kerr effects and new concept of future magneto-optical materials

The magneto-optical effects observed using polarised light can be divided into two categories: Faraday and Kerr effects, which are performed by the transmission and reflection modes, respectively. When linearly polarised light rotates because of transmission through a material under the magnetic field, the phenomenon is called Faraday rotation. When the rotational change in linearly polarised light occurs owing to the reflection of the light by the material under a magnetic field, the phenomenon is termed Kerr rotation. In the case of circularly polarised light, Faraday ellipticity or MCD refers to the difference in absorption of light transmitted through materials under magnetic fields between right- and left-circularly polarised light (Fig. 2). On the other hand, Kerr ellipticity is the difference in amounts of right- and left-circularly polarised light reflected from the material under a magnetic field (Fig. 2).

Experimentally, Kerr ellipticity measurements can be performed as shown in Fig. 3. Circularly polarised light generated by passing through both a polariser and a photoelastic modulator (PEM) is irradiated on a material under a magnetic field, and the reflected light is monitored with a photomultiplier (PMT). The difference between the right- and left-circularly

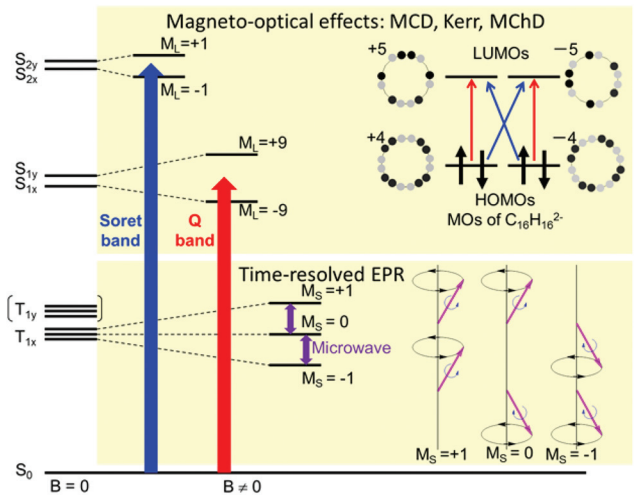


Fig. 1 Summary of the spectroscopies performed under a magnetic field.

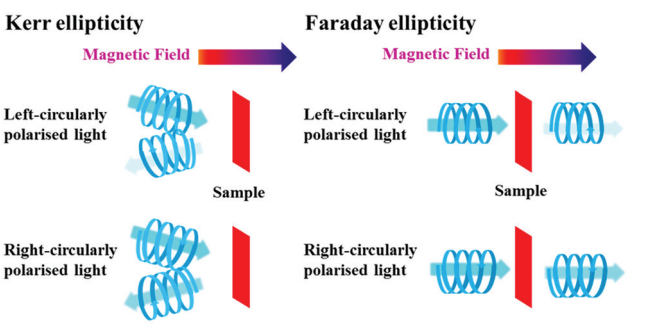


Fig. 2 Difference between the Kerr ellipticity (left) and the Faraday ellipticity (right).

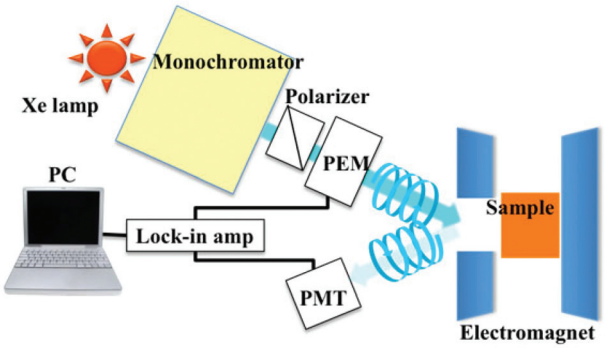


Fig. 3 A block diagram of a typical setup for Kerr ellipticity measurements.

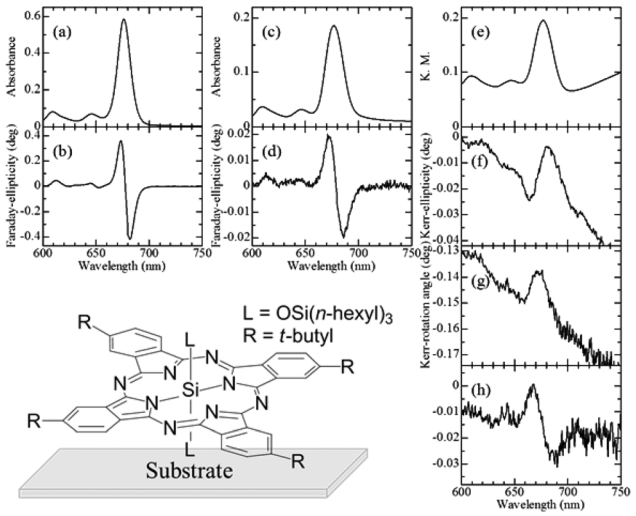


Fig. 4 (a) Electronic absorption and (b) MCD spectra of $SiPc(OTHS)_2$ in toluene; (c) diffuse transmission and (d) MCD Faraday ellipticity spectra of a $SiPc(OTHS)_2$ film on a glass substrate; (e) diffuse reflectance, (f) Kerr ellipticity, and (g) Kerr rotation spectra of a $SiPc(OTHS)_2$ film on a Ni substrate; (h) a dispersion-type spectral pattern was reproduced by the linear combination of the (f) Kerr ellipticity and (g) Kerr rotation spectra. The molecular structure of a $SiPc(OTHS)_2$ film on an inorganic substrate is shown in the bottom left. The diagrams were adapted from ref. 10.

polarised light is amplified by a lock-in amplifier connected to the PEM, which alternately produces right- and left-circularly polarised light.

Molecular magneto-optical effects can readily be observed in diluted sample solutions in the transmission mode. Thus, molecular Faraday effects have been investigated using MCD.[8] Further, a number of MCD-based studies have been performed on porphyrinic compounds in order to clarify their electronic properties. However, in order to be able to functionalise molecules for practical applications, the molecules must be manufactured in the form of solid materials. Thus, the Kerr effects of molecular materials are of greater significance; however, only a handful of reports have described the molecular Kerr phenomenon, in contrast to the numerous studies on MCD. Two reports related to the Kerr effect in cast films of porphyrinic compounds appeared in 2009.[9,10] Fronk and coworkers determined the Kerr effect parameter, $Q$, and the Voigt constant of cast films of vanadyl phthalocyanine (VOPc) and copper phthalocyanine (CuPc).[9] In the other report, Ishii and coworkers described the magnetic hysteresis of ditrihexylsiloxy (tetra-*tert*-butyl-phthalocyanato)silicon ($SiPc(OTHS)_2$) on ferromagnetic substrates; this phenomenon was observed for the first time at room temperature using Kerr spectroscopy.[10] Here, bulky substituents were introduced into SiPc in order to prevent the aggregation and direct interaction with the ferromagnetic substrates. Thus, the sharp Q absorption band was very useful for elucidating the relationship between the transmission and reflection modes. The sharp Q absorption band and the dispersion-type MCD Faraday A term of $SiPc(OTHS)_2$ on a glass substrate obtained using transmission spectroscopy are observed (Fig. 4). The sharp Q absorption band is comparable to that observed in a toluene solution, which indicates that the desired monomeric properties are retained even in the solid-film form, owing to the bulky substituents.

The electronic absorption and ellipticity spectra of a $SiPc(OTHS)_2$ film on a Ni substrate were obtained in the reflection mode. Despite the similarity between the absorption spectrum measured in the transmission mode and that measured in the reflection mode, the Kerr ellipticity spectrum obtained in the reflection mode was substantially different from the MCD spectrum obtained using the transmission mode. An analysis of the difference between the Faraday and Kerr effects follows the off-diagonal element of permittivity, which is expressed by $\varepsilon_{xy} = \varepsilon'_{xy} + i\varepsilon''_{xy}$.[11] In the transmission mode, MCD is proportional to $(n\varepsilon'_{xy} + \kappa\varepsilon''_{xy})/(n^2 + \kappa^2)$, where $n$ and $\kappa$ are the refractive index and the optical quenching, respectively. As the $\kappa$ value is negligible, MCD is determined only by $\varepsilon'_{xy}$. On the other hand, in the reflection mode, $\varepsilon''_{xy}$ is a contributing factor to the Kerr ellipticity. Therefore, the Kerr ellipticity spectrum is different from the MCD spectrum. When the Kerr ellipticity and the Kerr rotation are combined linearly, the MCD observed in the transmission mode can indeed be reproduced (Fig. 4h).

In the Kerr-ellipticity spectrum of the $SiPc(OTHS)_2$ film on a $SrO{\cdot}6Fe_2O_3$ substrate (Fig. 5), the integral-type spectral shape for $SiPc(OTHS)_2$ can be clearly seen in addition to the Kerr ellipticity signals arising from the $SrO{\cdot}6Fe_2O_3$ substrate. To investigate magnetic field effects, magnetic-field dependence of the Kerr ellipticity of solid films of $SiPc(OTHS)_2$ on ferromagnetic $SrO{\cdot}6Fe_2O_3$ was studied. The Kerr ellipticity of a $SiPc(OTHS)_2$ film on an Al substrate increased in proportion to the strength of the externally applied magnetic field; this behaviour is characteristic of diamagnetic materials. On the other hand, in the case of $SiPc(OTHS)_2/SrO{\cdot}6Fe_2O_3$, the magnetic-field dependence of the Kerr ellipticity signal due to $SiPc(OTHS)_2$ showed both hysteretic and nonsaturation effects. Further, the remanence and coercivity properties resembled those of the $SrO{\cdot}6Fe_2O_3$ substrate. It is believed that these interesting magneto-optical properties observed in the $SiPc(OTHS)_2/SrO{\cdot}6Fe_2O_3$ hybrid exist as a blend of the properties of the individual entities; the remanence and coercivity properties come from the ferromagnetic $SrO{\cdot}6Fe_2O_3$ substrate,

 

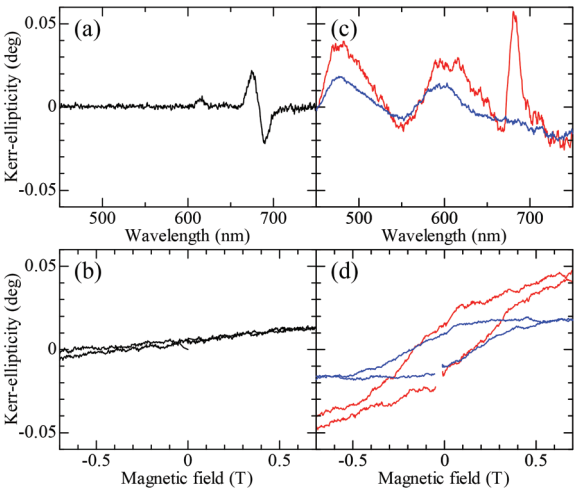


**Fig. 5** Kerr ellipticity spectra of $SiPc(OTHS)_2$ films on Al (a) and $SrO{\cdot}6Fe_2O_3$ (c: red lines) substrates; magnetic-field dependences of Kerr ellipticity of the $SiPc(OTHS)_2$ films on Al (b: 675 nm) and $SrO{\cdot}6Fe_2O_3$ (d: 680 nm, red lines) substrates; a Kerr ellipticity spectrum of the $SrO{\cdot}6Fe_2O_3$ substrate (c: blue line); a magnetic field dependence of Kerr-ellipticity of the $SrO{\cdot}6Fe_2O_3$ substrate (d: blue line, 480 nm). The diagrams were adapted from ref. 10.

while the nonsaturation effect derives from the diamagnetic $SiPc(OTHS)_2$ film.

The success in admixing diamagnetic porphyrinic compounds and ferromagnetic materials provides an insight into the development of new molecular magneto-optical devices based on the concept described in Fig. 6. By depositing porphyrins or phthalocyanines onto an appropriate magnetic substrate, the on/off switching of the magneto-optical effects of each sample spot can be controlled by laser irradiation at specific wavelengths. Thus, a logical optical memory that can overcome the memory-capacity dependence on the diffraction limit of light can be created.

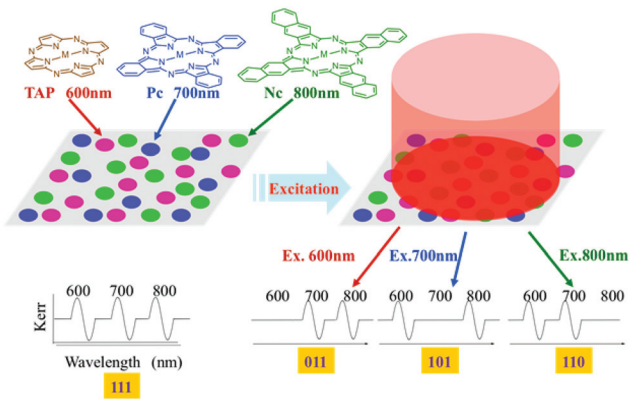


**Fig. 6** A novel molecular magneto-optical memory constructed from a combination of TAP (Q band, 600 nm), Pc (Q band, 700 nm), and Nc (Q band, 800 nm) that are deposited onto each magnetic domain of an appropriate magnetic substrate. A magneto-optical signal of type (1,1,1) is induced by an externally applied magnetic field. Light irradiation at 600 nm turns off the magneto-optical effect of the TAP spot owing to the thermomagnetic effect. Thus, a (0,1,1) signal is created. $2^N$ bits of information may be stored in the memory when $N$ kinds of dyes are used. The diagram was adapted from ref. 10.

## TREPR evaluations of the excited triplet states of low symmetry TAP derivatives

Upon light excitation, porphyrinic compounds undergo intersystem crossing (ISC) from the $S_1$ state to the $T_1$ state. The energy splitting in the $T_1$ state, ZFS, reflects useful electronic information, such as the anisotropy of the magnetic dipole–dipole interaction and SOC. EPR is appropriate for detecting the ZFS of the $\pi$–$\pi^*$ excited states;[12] this is not possible using other conventional methods.

The ISC is driven by the SOC that is dependent mainly on the type of the central atom. The ISC from the $S_1$ state may selectively go to each triplet sublevel, that is, to the $x$, $y$, and $z$ sublevels in the $T_1$ state, depending on the SOC of the porphyrinic compound. The TREPR technique is very useful for studying the $T_1$ states not only for detecting molecules with short excited-state lifetimes but also for evaluating spin-selective ISCs.[13,14] When a Zn porphyrin is randomly oriented in a glassy matrix, an AAA/EEE polarisation pattern is seen because of the selective ISC to the $z$ sublevel of the $T_1$ state, as shown in Fig. 7.

One way to perform TREPR measurements is by using a modified continuous-wave EPR spectrometer, so that it can run in a time-resolved mode (Fig. 8).[14] For this purpose, a digital oscilloscope and/or a boxcar integrator are employed instead of a magnetic field modulation, as shown in Fig. 8. After the pulsed-laser excitations, the TREPR spectra can be obtained by measuring the TREPR signals at an arbitrary time with scanning magnetic fields. When the TREPR signals are

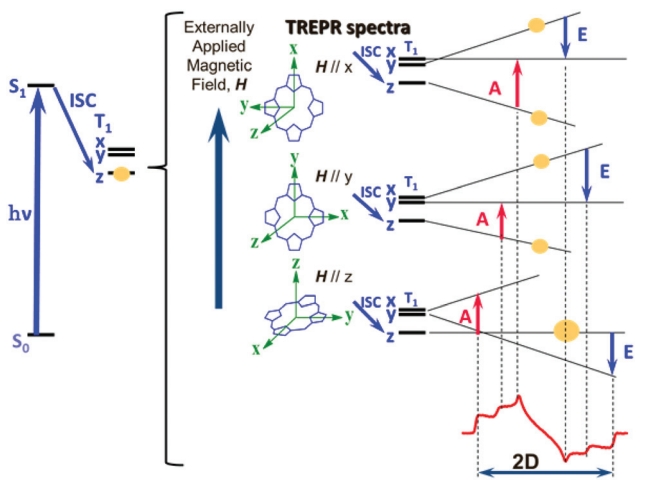


**Fig. 7** A qualitative explanation of the TREPR spectrum of the $T_1$ zinc porphyrin. When a Zn porphyrin is randomly oriented in a glassy matrix, the selective population of the $z$ sublevel results in an AAA/EEE polarisation pattern. Here, A and E denote the absorption and emission of microwaves, respectively.

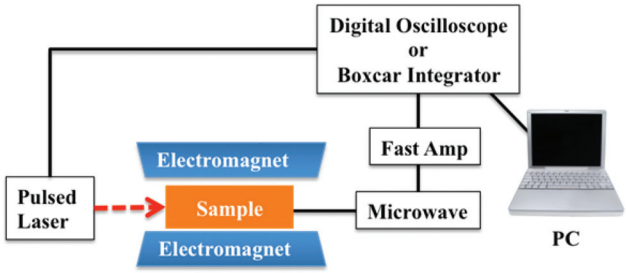


Fig. 8 A block diagram of the setup used for the TREPR measurements.

measured before spin-lattice relaxation, A or E polarisation owing to the spin-selective ISC can be seen. In addition, conventional EPR parameters, such as the ZFS and the $g$ values, can also be evaluated.

Kobayashi, Ishii and coworkers found that the ZFS parameter $D$ was correlated to the $\Phi_\Delta$ value in the case of low-symmetry tetraazaporphyrin (TAP) derivatives (Scheme 1).[15] They reached this conclusion on the basis of both the formation of singlet oxygen ($^1\Delta_g$) *via* the $T_{1y}$ state and the energy evaluation of $T_{1y}$ using the ZFS parameter $D$. As shown in Fig. 9, the TREPR signals of low-symmetry **1Zn** display an AAA/EEE polarisation pattern because of the ISC to the $z$ sublevel. This selective ISC results from the $z$ component of the SOC between the $d_{xz}$ and $d_{yz}$ orbitals of the zinc atoms that are mixed with the $\pi^*$ orbitals of the porphyrin ligand.[16] In the case of $T_1$ porphyrinic complexes, the ZFS parameter $D$ is influenced by not only the magnetic dipole–dipole interactions between the highest occupied molecular orbital (HOMO) and the lowest unoccupied molecular orbital (LUMO), $D_{SS}$, but also the SOC between the $T_{1x}$ and $T_{1y}$ states, $D_{SOC}$, where the $T_{1x}$ and $T_{1y}$ states are generally called the $T_1$ and $T_2$ states, respectively. That the deviation in the observed $g_{zz}$ values of the Zn series (<0.006) was negligible indicates that the ZFS in the Zn series mainly originates from the magnetic dipole–dipole interactions, and that the SOC between the $T_{1x}$ and $T_{1y}$ states has little effect. In the Zn series, the value of the ZFS parameter $D$ representing the anisotropic magnetic dipole–dipole interaction towards the out-of-plane ($z$) axis tends to decrease in order with an increase in the number of benzo-ring substitutions. However, the ZFS parameter $E$ values representing the anisotropic magnetic dipole–dipole interactions towards the in-plane ($x$ and $y$) axes do not follow such a trend (Table 1).

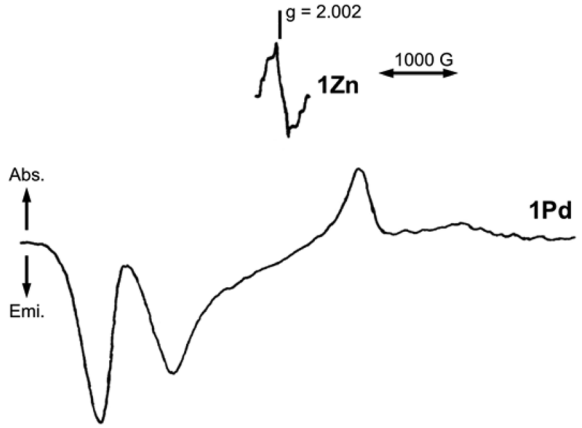


Fig. 9 TREPR spectra of **1Zn** (top) and **1Pd** (bottom). The diagrams were adapted from ref. 15.

It is interesting to note the temperature dependence of the $D$ value specific to **2AdZn**. While the temperature does not affect the $D$ values of the other Zn complexes, that of **2AdZn** decreases as the temperature rises. Half-point charge calculations performed for **2AdZn** reveal that the calculated $D$ value of the $T_{1y}$ state is smaller than that of the $T_{1x}$ state; thus the decrease in the $D$ value should be caused by the change in the population between the $T_{1x}$ and the nearby $T_{1y}$ states. The observed $D$ value ($D_{obs}$) can be expressed in terms of the energy difference between the $T_{1x}$ and $T_{1y}$ states ($\Delta E_{TT}$) according to the following equations:

$$D_{obs}\ (\mathbf{2AdZn}) = \{D(T_{1x})P_1 + D(T_{1y})P_2\}/(P_1 + P_2) \quad (1a)$$

$$P_1 = \exp(\Delta E_{TT}/2kT), P_2 = \exp(-\Delta E_{TT}/2kT) \quad (1b)$$

Assuming that $D(T_{1x})$ is the $D$ value at 20 K, the experimental results were well-reproduced by the $D_{obs}$ value derived using

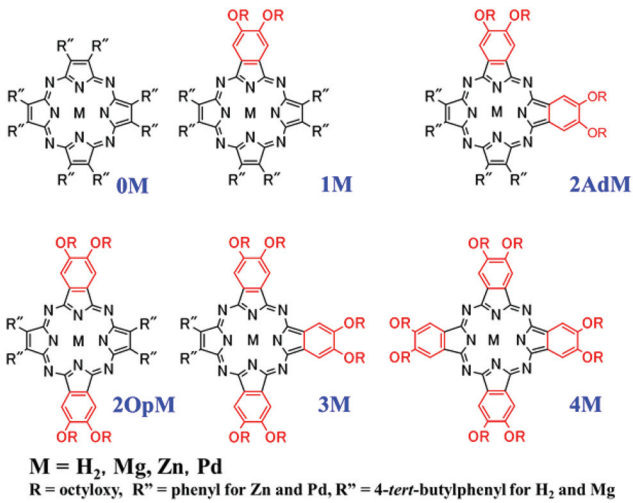


Scheme 1 Molecular structures of Zn, Pd, and metal-free TAPs with fused benzo-ring substituents at different positions.

Table 1 The observed EPR parameters, $D_{obs}$, $E_{obs}$, and $g_{zz}$, as well as the calculated ZFS parameters, $D_{calcd}$ and $E_{calcd}$[15]

| Compd | $D_{obs}$/ $10^{-3}$ cm$^{-1}$ | $D_{calcd}$/ $10^{-3}$ cm$^{-1}$ | $\lvert E_{obs}\rvert$/ $10^{-3}$ cm$^{-1}$ | $\lvert E_{calcd}\rvert$/ $10^{-3}$ cm$^{-1}$ | $g_{zz}$ |
|---|---|---|---|---|---|
| **0Zn** | 29.0 | 28.0 | 5.33 | 3.20 | 1.999 |
| **1Zn** | 26.0 | 25.5 | 4.00 | 3.80 | 1.999 |
| **2AdZn** | 26.8 | 26.5 | 8.54 | 10.8 | 1.998 |
| **2OpZn** | 23.5 | 21.3 | 5.17 | 4.76 | 1.999 |
| **3Zn** | 22.8 | 21.3 | 2.92 | 4.49 | 1.999 |
| **4Zn** | 21.8 | 21.1 | 6.09 | 4.26 | 1.995 |
| **1Pd** | −221 | — | 5.00 | — | 1.968 |
| **2OpPd** | −141 | — | 0 | — | 1.985 |
| **3Pd** | −215 | — | 0 | — | 1.971 |

eqn (1a). According to eqn (1a) and (1b), the $\Delta E_{TT}$ and $D(T_{1y})$ values were $2.5 \times 10^2$ and $2.3 \times 10^{-2}$ $cm^{-1}$, respectively, which indicates that the $T_{1y}$ energy of **2AdZn** is very close to its $T_{1x}$ energy.

In contrast to the Zn series, the TREPR spectra of **1Pd**, **2OpPd**, and **3Pd** exhibited EEE/AAA polarisation patterns, and very-high-intensity E signals were observed at the lowest magnetic field assigned as $\Delta m_s = 2$ (Fig. 9). When compared to the Zn complexes, the most striking difference in the case of the TREPR data of the Pd complexes is that their $|D|$ values are much larger. The most significant reason for these larger $|D|$ values for the Pd complexes is the $z$ component of the large SOC between the $T_{1x}$ and $T_{1y}$ states,[17] where $\Delta E_{TT}$ can be evaluated quantitatively. According to eqn (2), the $D_{obs}$ value for the Pd complexes can be expressed as the sum of the $D_{SS}$ and $D_{SOC}$ values.

$$D_{obs}\ (\mathrm{Pd}) = D_{SS} + D_{SOC} \quad (2)$$

Assuming that the $D_{SS}$ values of the Pd complexes are the same as the $D$ values observed for the corresponding Zn complexes, the $D_{SOC}$ values were found to be −0.247, −0.166, and −0.238 $cm^{-1}$ for **1Pd**, **2OpPd**, and **3Pd**, respectively. Following the second-order perturbation principle, the $D_{SOC}$ value can be expressed with respect to the $Z$ value (eqn (3)), which originates from the SOC constant, $\xi$, and the $C_{dyz}$ and $C_{dxz}$ MO coefficients.[18,19]

$$D_{SOC} = -Z^2/4\Delta E_{TT} \quad (3a)$$

$$\mathrm{i}Z = \xi C_{dyz}\ C_{dxz}\ \langle d_{yz}|l_z|d_{xz}\rangle \quad (3b)$$

Thus, the $\Delta E_{TT}$ values for **1Pd**, **2OpPd**, and **3Pd** were experimentally found to be 850 ± 300, 1300 ± 400, and 880 ± 300 $cm^{-1}$, respectively.

While the TREPR technique can be used to evaluate the $\Delta E_{TT}$ values, the electronic absorption and MCD measurements provide data on the difference in the energies of the $S_{1x}$ and $S_{1y}$ states, $\Delta E_{SS}$.[15] As shown in Fig. 10, the $\Delta E_{SS}$ and $\Delta E_{TT}$ values obtained from the MCD and TREPR measurements, respectively, suggest that there is a systematic correlation between $\Delta E_{SS}$ and $\Delta E_{TT}$.

Low-symmetry TAP derivatives have been investigated to explore the possibility of accessing compounds with strong absorptions at longer wavelengths, as they are useful for developing materials for use in many applications, including the photochemical generation of singlet oxygen in PDT.[20] As described earlier, the $T_1$ state can be accessed through the ISC from $S_1$ to $T_1$, which is generally triggered in porphyrinic compounds by the SOC of a heavy atom; this is known as the "heavy atom effect". The subsequent transfer of energy from the $T_1$ state of the porphyrinic compound to the triplet molecular oxygen generates a singlet oxygen. The heavy atom effect is manifested through the shorter fluorescence lifetimes ($\tau_f$) observed for the ZnTAP derivatives compared with those of the corresponding MgTAP derivatives (Table 2).[21] The shorter lifetimes result from the ISC being more accessible, which results in the easier production of singlet oxygen. On the other hand,

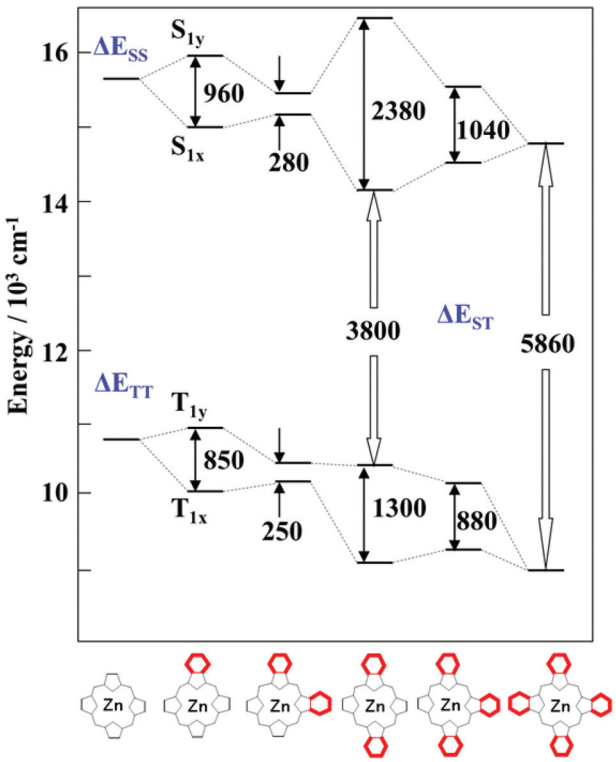


**Fig. 10** The $\Delta E_{SS}$ and $\Delta E_{TT}$ values obtained by the MCD and TREPR measurements. The diagram was adapted from ref. 15.

**Table 2** Fluorescence lifetimes ($\tau_f$) and singlet oxygen yields ($\Phi_\Delta$) observed for Zn, Mg, and metal-free TAP derivatives[21]

| Compounds | $\tau_f$/ns | $\Phi_\Delta$ |
|---|---|---|
| **1Zn** | 1.5 | 0.62 |
| **2AdZn** | 1.1 | 0.49 |
| **2OpZn** | 2.2 | 0.60 |
| **3Zn** | 1.5 | 0.55 |
| **4Zn** | 3.4 | 0.43 |
| **1Mg** | 2.5 | 0.27 |
| **2AdMg** | 3.8 | 0.18 |
| **2OpMg** | 2.6 | 0.24 |
| **3Mg** | 3.4 | 0.20 |
| **4Mg** | 6.5 | 0.14 |
| **1H$_2$** | 1.7 | 0.23 |
| **2AdH$_2$** | 0.081 | 0.010 |
| **2OpH$_2$** | 2.4 | 0.50 |
| **3H$_2$** | 4.2 | 0.27 |
| **4H$_2$** | 6.1 | 0.14 |

despite the strong involvement of the heavy atom, the singlet oxygen yield of **2OpH$_2$** was found to be higher than that observed for **4Zn** (Table 2).

A comparison of the isomers suggests that the change in positions of the two benzo-rings results in an extremely large difference in the singlet oxygen yields of **2AdH$_2$** and **2OpH$_2$**. As shown in Fig. 11, the generation of a singlet oxygen *via* the $S_{1x} \rightarrow T_{1y}$ ISC followed by the energy transfer to triplet molecular oxygen occurs more readily in a system in which the energy gap between the $S_{1x}$ and $T_{1y}$ states is small. The noticeably large $Q_x$–$Q_y$ band splitting in the case of **2OpH$_2$** would result

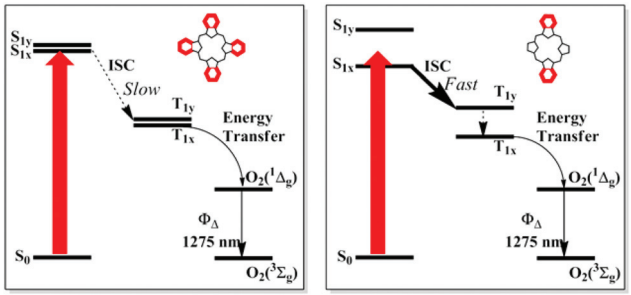


**Fig. 11** Singlet oxygen generation mechanisms in **4M** and **2OpM**.

in a smaller energy gap between the $S_{1x}$ and $T_{1y}$ states. This would consequently increase the singlet oxygen yield. The better performance of $\mathbf{2OpH_2}$ in comparison with that of **4Zn** makes the former better suited for PDT applications, as metal-free porphyrinic compounds are generally less toxic than their metal-containing counterparts are.

## MCD evaluations of prototropic tautomers of low symmetry TAP derivatives

A number of MCD studies on the effect of lowering the symmetry of metal-free TAPs have been carried out not only to clarify the degeneracy of the excited singlet states in these compounds but also to detect the tautomers generated by the positioning of the two pyrrole protons around the N4 ring.[22] As shown in Fig. 12, the systematic introduction of fused benzo-rings in metal-free TAPs results in "prototropic" tautomerism between X and Y, which is created by the difference in the positions of the two pyrrole protons with respect to the benzo-rings.

The electronic absorption spectra of $\mathbf{2AdH_2}$ and $\mathbf{2OpH_2}$ (Fig. 10) reveal the typical splitting of the $Q_x$ and $Q_y$ bands, which correspond to the characteristic Faraday B terms of the opposite sign in the MCD spectra. In contrast to these compounds, $\mathbf{1H_2}$ and $\mathbf{3H_2}$ display three absorption bands in the Q-band region; these correspond to one pseudo-Faraday A term and two Faraday B terms in the MCD spectra. The pseudo-A term of the single Q band positioned in the middle is constituted by the positive and negative B terms, which originate from the $Q_y$ (higher energy) and $Q_x$ (lower energy) bands, respectively. Configuration interaction (CI) calculations were attempted for both $\mathbf{1H_2}$ and $\mathbf{3H_2}$ to elucidate the pseudo-A terms and to further assess the possibility of the existence of X ($\mathbf{1H_2X}$ and $\mathbf{3H_2X}$) and Y ($\mathbf{1H_2Y}$ and $\mathbf{3H_2Y}$) tautomers.

While the Q bands at 721 and 603 nm as calculated for the $\mathbf{1H_2X}$ model in $\mathbf{1H_2}$ fit reasonably well with the observed $Q_x$ and $Q_y$ bands at 701 and 598 nm, respectively, the calculation for the $\mathbf{1H_2Y}$ model resulted in nearly degenerate Q bands (656 and 654 nm), which indicates the existence of the pseudo-A term, as observed at 653 nm. A similar result was obtained for the calculations for the $\mathbf{3H_2X}$ and $\mathbf{3H_2Y}$ models in $\mathbf{3H_2}$. Thus, the X and Y tautomers generated by the different positioning of the two pyrrole protons are present in $\mathbf{1H_2}$ and $\mathbf{3H_2}$ at room temperature.

## Magneto-chiral dichroism of porphyrinic compounds

MChD is a phenomenon in which the absorbance of a chiral molecule is dependent upon the direction of the magnetic field.[23] Fig. 13 illustrates opposite MChD effects in a pair of enantiomers upon the application of parallel and antiparallel magnetic fields. Compounds that show both circular dichroism (CD) and MCD signals are expected to be MChD active, although the origins of the two are totally different; CD is

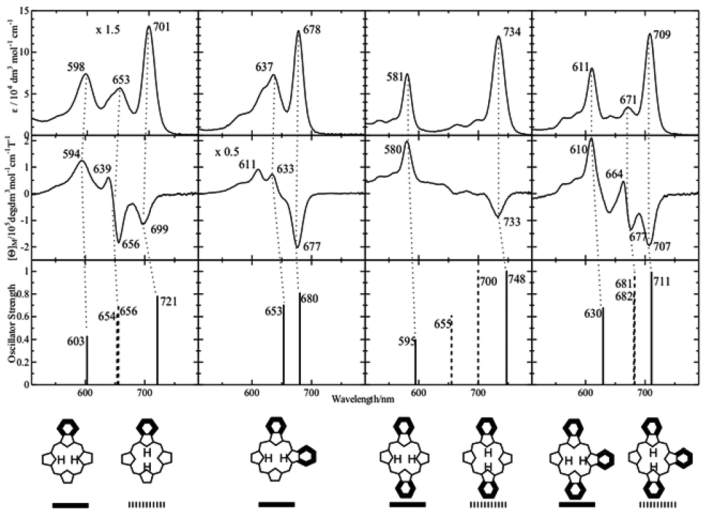


**Fig. 12** Electronic absorption (upper), MCD (middle), and CI calculation (lower) spectra of low-symmetry $H_2$TAP derivatives. The X tautomers are indicated by the solid lines, whereas the Y tautomers are indicated by the broken lines. The diagrams were adapted from ref. 22.

 

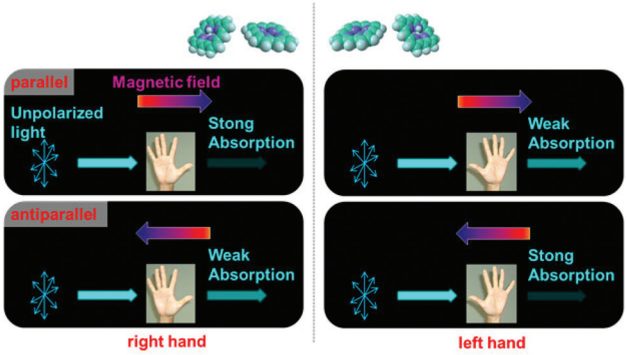


Fig. 13 Illustration of the MChD phenomenon showing the opposite MChD effects of a pair of enantiomers, which are represented by hands instead of molecules; when a parallel magnetic field is applied, the right-handed enantiomer exhibits stronger absorption than does the left-handed one; the effect is reversed when an antiparallel magnetic field is applied.

based on molecular chirality, whereas MCD is owing to the Zeeman effect. The intensity of MChD has a strong correlation with the transition electric dipole, transition magnetic dipole, and transition electric quadrupole moments, in addition to the magnetic dipole moments between the excited states. Since the CD intensity corresponds to an imaginary part of the cross product of the transition electric dipole and the transition magnetic dipole moments, and because the MCD intensity correlates with the transition electric dipole moment and the magnetic dipole moment between the excited states, $g_{MChD}$ can be roughly estimated as the product of $g_{CD}$ and $g_{MCD}$.

Fig. 14 shows one way of making MChD measurements. The magnetic field that is applied to the sample can be set parallel or antiparallel with respect to the light direction. Monochromatic light is made to pass through an optical chopper, and is amplified by a photomultiplier connected to a lock-in amplifier. In this manner, the MChD spectra can be obtained.

Early investigations of the MChD phenomenon in europium(III) complexes with the luminescent $5D_0 \rightarrow 7F_{1,2}$ transition were mainly motivated by the fact that the MCD is intensified by d- or f-orbital-based degeneracy and the angular momentum of the metals.[23] In organic compounds, the orbital angular momentum can be intensified by the size of the π-conjugated systems. The exciton chirality that contributes to the strong CD signal arises when two transition electric dipole moments of organic chromophores are twisted in the chiral dimer. MCD-active organic molecules that display exciton chirality should therefore exhibit MChD properties.

While there have not been many studies on the occurrence of MChD in organic compounds, it is critical to gain a fundamental understanding of the homochirality in living things because organic molecules, in particular, amino acids and sugars, are biologically relevant as the building blocks of biomolecules. The phenomenon of MChD may lead to an understanding of the origin of the homochirality of life. For example, it may lead to an explanation of the chiral distribution of L-amino acids and D-sugars, as well as the development of new methods for the photochemical asymmetric synthesis of industrially important chemical compounds.

In 2011, Ishii and coworkers reported observing MChD in an organic compound using chiral J-aggregates of *meso*-tetrakis(4-sulfonatophenyl)porphine ($H_4TPPS_4$) that was obtained by treating the monomer with chiral tartaric acid.[24] In a follow-up report, they described the MChD properties of Zn chlorins (ZnChl),[25] which are related to magnesium-containing chlorins that function as light-harvesting antennae during photosynthetic processes (Fig. 15). As shown in Fig. 15, monomeric ZnChl shows a $Q_x$ (0,0) band at 581 nm, a $Q_y$ (1,0) band at 611 nm, and a $Q_y$ (0,0) band at 658 nm. The MCD spectrum of the monomer shows the Faraday B term, indicating the nondegeneracy of the excited states. Upon the formation of the J-aggregates, a large red shift in the $Q_y$ band to 729 nm was noticed, in contrast to the small shift in the $Q_x$ bands. The red shift of the $Q_y$ band is due to the exciton interactions between

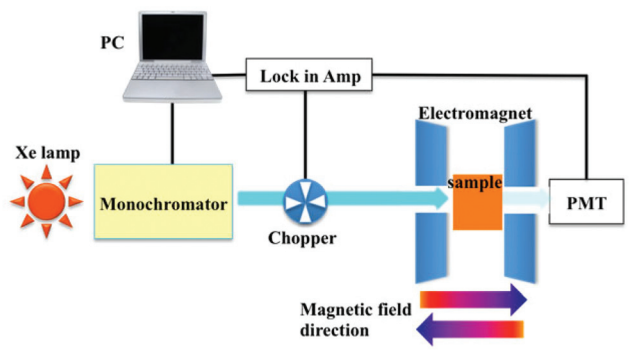


Fig. 14 A block diagram of the setup used for the MChD measurements.

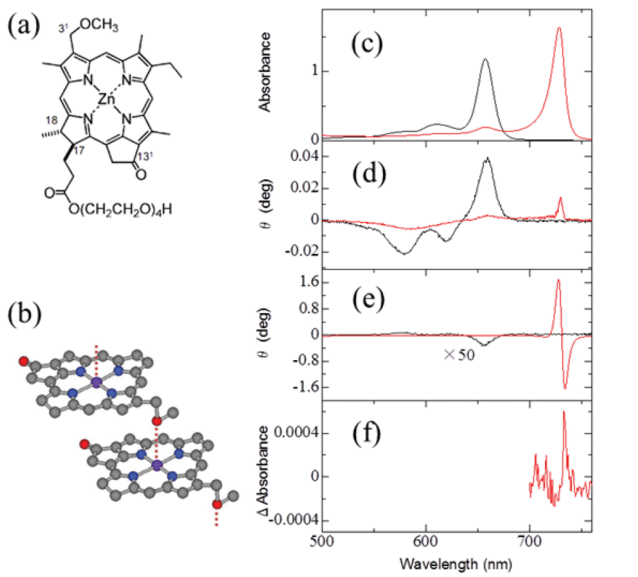


Fig. 15 Molecular structures of (a) ZnChl and (b) its J-aggregates; (c) electronic absorption, (d) MCD, (e) CD, and (f) MChD of the J-aggregates of ZnChl (red) and monomeric ZnChl (black). The diagrams were adapted from ref. 25.

the ZnChl constituents; this results in an increase in the separation energy between the $Q_x$ and $Q_y$ bands. This would also lead to the MCD B-term of the $Q_y$ band of the J-aggregates being relatively weak. The chirality of the J-aggregates was confirmed by the CD spectrum, which showed an intense inverse-S-shaped signal at the $Q_y$ band, in contrast to the monomeric form, which shows a very weak CD signal at a shorter wavelength, owing to the chiral moiety in it. The chirality of the J-aggregates derives from the exciton chirality, because of the twisted configuration between the large electric transition dipole moment of each chromophore.[26] Measuring the difference in the absorbances under parallel and antiparallel magnetic fields gives a positive MChD signal that peaks at 733 nm; this was found to be similar to the product of the CD and MCD spectra. Very recently, Jiang and coworkers reported the MChD properties of the triple-decker complex, $Dy_2[Pc(OBNP)_4](TClPP)_2$, which exhibits single-molecule magnet (SMM) behaviour.[27] The complex comprises two porphyrin moieties and one phthalocyanine moiety connected by two dysprosium atoms. The high-intensity CD signal of this complex originates from the chirality that is induced by the presence of the binaphthyl substituents in the phthalocyanine ligand.

## Conclusions

In this perspective, various spectroscopies performed under a magnetic field were reviewed, while focusing on the molecular functions. A Kerr spectroscopic study of $SiPc(OTHS)_2$ coupled with a ferromagnetic $SrO{\cdot}6Fe_2O_3$ substrate revealed that the magnetic hysteresis of molecular Kerr ellipticity exists even at room temperature. This can lead to a novel molecular functionality that can be used to fabricate molecular memory devices. A TREPR study of low-symmetry TAPs elucidated the relationship between molecular symmetry and the $\Phi_\Delta$ values. This should allow for greater flexibility in the design of singlet-oxygen generators such as PDT photosensitisers. Finally, a MChD study investigated porphyrinic compounds with the homochirality of life in focus. Thus, molecular spectroscopies performed under a magnetic field can open up novel possibilities in science and technology, in addition to elucidating the molecular electronic structures of various compounds.

## Acknowledgements

This work was supported by a Grant-in-Aid for Scientific Research (Category B no. 24350065) from the Ministry of Education, Culture, Sports, Science & Technology in Japan. We thank Japan Society for the Promotion of Science (JSPS) for the research fellowship granted to Y. M.

## Notes and references

1 O. T. G. Jones, in *The Porphyrins*, ed. D. Dolphin, Academic Press, New York, 1979, vol. 6, Part A, pp. 179–228; L. F. Ten Eyck, in *The Porphyrins*, ed. D. Dolphin, Academic Press, New York, 1979, vol. 6, Part B, pp. 445–471; B. R. Crane, L. M. Siegel and E. D. Getzoff, *Science*, 1995, **270**, 59.

2 T. Patrice, *Photodynamic Therapy*, The Royal Society of Chemistry, London, 2004; J. G. Moser, *Photodynamic Tumor Therapy: 2nd and 3rd generation Photosensitizers*, Harwood Academic Publishers, Amsterdam, 1998; I. Rosenthal and E. Ben-Hur, in *Phthalocyanines, Properties and Applications*, ed. C. C. Leznoff and A. B. P. Lever, VCH Publishers, New York, 1989.

3 B. M. Hoffman and J. A. Ibers, *Acc. Chem. Res.*, 1983, **16**, 15; J. Simon, in *Molecular Semiconductors*, ed. J.-J. Andre, Springer, Berlin, 1985; P. Turek, P. Petit, J.-J. Andre, J. Simon, R. Even, B. Boudjema, G. Guillaud and M. Maitrot, *J. Am. Chem. Soc.*, 1987, **109**, 5119; D. Whörle and D. Meissner, *Adv. Mater.*, 1991, **3**, 129.

4 J. Rostalki and D. Meissner, *Sol. Energy Mater. Sol. Cells*, 2000, **63**, 37; R. Koeppe, N. S. Sariciftci, P. A. Troshin and R. N. Lyubovskaya, *Appl. Phys. Lett.*, 2005, **87**, 244102; D. Wohrle, L. Kreienhoop and D. Schlettwein, in *Phthalocyanines, Properties and Applications*, ed. C. C. Leznoff and A. B. P. Lever, New York, 1996, vol. 4, ch. 6, pp. 219–284.

5 R. O. Loutfy, A. M. Hor, C. K. Hsiao, G. Baranyi and P. Kazmaier, *Pure Appl. Chem.*, 1988, **60**, 1047; K. Y. Law, *Chem. Rev.*, 1993, 449.

6 G. de la Torre, P. Vazquez, F. Agullo-Lopez and T. Torres, *Chem. Rev.*, 2004, **104**, 3723; S. R. Flom, in *The Porphyrin Handbook*, ed. K. M. Kadish, K. M. Smith and R. Guilard, Academic Press, New York, 2003, vol. 19, p. 179; H. S. Nalwa and J. A. Shirk, in *Phthalocyanines, Properties and Applications*, ed. C. C. Leznoff and A. B. P. Lever, 1996, New York, vol. 4, ch. 3, pp. 79–118.

7 M. Gouterman, in *The Porphyrins*, ed. D. Dolphin, Academic Press, New York, 1978, vol. 3, Part A, pp. 1–156; J. C. Sutherland, in *The Porphyrins*, ed. D. Dolphin, Academic Press, New York, 1978, vol. 3, Part A, pp. 225–246; S. B. Piepho and P. N. Schatz, *Group Theory in Spectroscopy: With Applications to Magnetic Circular Dichroism*, John Wiley and Sons, New York, 1983; J. Mack, Y. Asano, N. Kobayashi and M. J. Stillman, *J. Am. Chem. Soc.*, 2005, **127**, 17697; J. Michl, *J. Am. Chem. Soc.*, 1978, **100**, 6801; J. Michl, *J. Am. Chem. Soc.*, 1978, **100**, 6812; J. Mack and N. Kobayashi, *Chem. Rev.*, 2011, **111**, 281; W. R. Browett and M. J. Stillman, *J. Comput. Chem.*, 1987, **8**, 241; J. Mack and M. J. Stillman, in *The Porphyrin Handbook*, ed. K. M. Kadish, R. M. Smith and R. Guilard, Academic Press, New York, 2003, vol. 16, ch. 103; M. J. Stillman and T. Nyokong, in *Phthalocyanines–Properties and Applications*, ed. C. C. Leznoff and A. B. P. Lever, VCH, New York, 1989, vol. 1, ch. 3; M. J. Stillman, in *Phthalocyanines-Properties and Applications*, ed. C. C. Leznoff and A. B. P. Lever, VCH, New York, 1993, vol. 3, ch. 5; J. Mack and M. J. Stillman, *Coord. Chem. Rev.*, 2001, **219–221**, 993; E. I. Solomon, T. C. Brunold, M. I. Davis, J. N. Kemsley, S.-K. Lee, N. Lehnert, F. Neese, A. J. Skulan, Y.-S. Yang and J. Zhou, *Chem. Rev.*, 2000, **100**, 235.

 

8 B. Holmquist, in *The Porphyrins*, ed. D. Dolphin, Academic Press, New York, 1978, vol. 3, Part A, pp. 249–269.
9 M. Fronk, B. Brauer, J. Kortus, O. G. Schmidt, D. R. T. Zahn and G. Salvan, *Phys. Rev. B: Condens. Matter*, 2009, **79**, 235305.
10 K. Ishii and K. Ozawa, *J. Phys. Chem. C*, 2009, **113**, 18897.
11 K. Sato, *Light and magnetism*, Asakura-Shoten, Tokyo (in Japanese), 1988.
12 J. A. Weil, J. R. Bolton and J. E. Wertz, *Electron Paramagnetic Resonance*, John Wiley and Sons, New York, 1994.
13 S. S. Kim and S. I. Weissman, *J. Magn. Reson.*, 1976, **24**, 167; N. Hirota and S. Yamauchi, in *Dynamics of Excited Molecules*, ed. K. Kuchitsu, Elsevier, Amsterdam, 1994, ch. 13; N. Hirota and S. Yamauchi, in *Dynamic Spin Chemistry*, ed. S. Nakagura, H. Hayashi and T. Azumi, Kodansha, Tokyo, 1998, ch. 7; N. V. Lebedeva, V. F. Tarasov, M. J. E. Resendiz, M. A. Garcia-Garibay, R. C. White and M. D. E. Forbes, *J. Am. Chem. Soc.*, 2010, **132**, 82; O. A. Krumkacheva, V. R. Gorelik, E. G. Bagryanskaya, N. V. Lebedeva and M. D. E. Forbes, *Langmuir*, 2010, **26**, 8971; N. J. Turro, M. H. Kleinman and E. Karatekin, *Angew. Chem., Int. Ed.*, 2000, **39**, 4436.
14 N. Hirota and S. Yamauchi, *J. Photochem. Photobiol., C*, 2003, **4**, 109.
15 H. Miwa, K. Ishii and N. Kobayashi, *Chem. – Eur. J.*, 2004, **10**, 4422.
16 J. H. van der Waals, W. G. van Dorp and T. J. Schaafsma, in *The Porphyrins*, ed. D. Dolphin, 1978, Academic Press, New York, vol. 4, ch. 3; W. G. van Dorp, W. H. Shoemaker, M. Soma and J. H. van der Waals, *Mol. Phys.*, 1975, **30**, 1701; K. Ishii, T. Ishizaki and N. Kobayashi, *J. Phys. Chem. A*, 1999, **103**, 6060; K. Ishii, S. Abiko and N. Kobayashi, *Inorg. Chem.*, 2000, **39**, 468.
17 J. A. Kooter, G. W. Canters and J. H. van der Waals, *Mol. Phys.*, 1977, **33**, 1545; W. H. Chen, K. E. Rieckhoff and E. M. Voigt, *Chem. Phys.*, 1985, **95**, 123; W. H. Chen, K. E. Rieckhoff and E. M. Voigt, *Chem. Phys.*, 1986, **102**, 193; W. H. Chen, K. E. Rieckhoff and E. M. Voigt, *Mol. Phys.*, 1986, **59**, 355; W. A. J. A. van der Poel, A. M. Nuijs and J. H. van der Waals, *J. Phys. Chem.*, 1986, **90**, 1537.
18 K. Ishii, Y. Ohba, M. Iwaizumi and S. Yamauchi, *J. Phys. Chem.*, 1996, **100**, 3839.
19 T. M. Dunn, *Trans. Faraday Soc.*, 1961, **57**, 1441.
20 K. Ishii, *Coord. Chem. Rev.*, 2012, **256**, 1556.
21 K. Ishii, H. Itoya, H. Miwa, M. Fujitsuka, O. Ito and N. Kobayashi, *J. Phys. Chem. A*, 2005, **109**, 5781.
22 K. Ishii, H. Itoya, H. Miwa and N. Kobayashi, *Chem. Commun.*, 2005, 4586.
23 G. L. J. A. Rikken and E. Raupach, *Nature*, 1997, **390**, 493.
24 Y. Kitagawa, H. Segawa and K. Ishii, *Angew. Chem., Int. Ed.*, 2011, **50**, 9133.
25 Y. Kitagawa, T. Miyatake and K. Ishii, *Chem. Commun.*, 2012, **48**, 5091.
26 M. Nakazaki, *Introduction to theory of optical rotation*, Baifukan, Tokyo, 1973; N. Harada and K. Nakanishi, *Circular Dichroic Spectroscopy-Exciton Coupling in Organic Stereochemistry*, Tokyo Kagaku Dojin, Tokyo, 1982.
27 K. Wang, S. Zeng, H. Wang, J. Dou and J. Jiang, *Inorg. Chem. Front.*, 2014, **1**, 167.